

Model and design of a double frequency piezoelectric resonator

Original

Model and design of a double frequency piezoelectric resonator / Bonin, Roberto; Zenerino, Enrico Cesare; Tonoli, Andrea; Amati, Nicola; Rapisarda, A.. - ELETTRONICO. - (2013). (Intervento presentato al convegno 6th ECCOMAS Thematic Conference on Smart Structures and Materials (SMART2013) tenutosi a Torino nel 24-26 giugno 2013).

Availability:

This version is available at: 11583/2509674 since:

Publisher:

Published

DOI:

Terms of use:

This article is made available under terms and conditions as specified in the corresponding bibliographic description in the repository

Publisher copyright

(Article begins on next page)

MODEL AND DESIGN OF A DOUBLE FREQUENCY PIEZOELECTRIC RESONATOR

Roberto Bonin¹, Enrico C. Zenerino¹, Andrea Tonoli¹, Nicola Amati¹, Alessandro Rapisarda²

¹ Politecnico di Torino

Department of Mechanical and Aerospace Engineering (DIMEAS) - Mechatronics Lab

Corso Duca degli Abruzzi, 24

10129, Torino, Italy

² Aviospace S.r.l.

Via Pier Carlo Boggio, 59/61

10138, Torino, Italy

e-mail of corresponding author: roberto.bonin@polito.it, web page: <http://www.lim.polito.it>

Key words: Piezoelectric materials, Energy harvesting.

Summary. *A novel design of a multifrequency mechanical resonator with piezoelectric materials for energy harvesting is presented. The electromechanical response is described by a finite element model, which predicts the output voltage and the generated power.*

1. Introduction

The studies on energy harvesting technologies from unused sources, like mechanical vibrations and wasted heat, have been noticeably increased during the last twenty years. Such interest arises from the request of renewable and environmentally “green” sources of energy in order to deal with the problem of pollution and global warming. Within all the various waste sources, the exploitation of mechanical vibrations results very promising because of its several applications in various fields like automotive, aerospace and railway technologies, and machine tools [1]. In particular, the energy harvesters excited by mechanical vibrations result particularly useful to power the sensors localized along the whole structure (car, train, space launcher, etc...), with the resulting severe reduction of the number of electrical current cables.

The vibration-based energy harvesters are developed by using three different transduction mechanisms: electromagnetic, electrostatic, and piezoelectric. In details, energy harvesters based on piezoelectric materials reveal themselves particularly promising in all the applications where small and compact dimensions and relatively low power are required [2]. Piezoelectric energy harvesters are commonly composed by a cantilever in the clamped-free configuration, which is bend by the action of external vibrations [3]. A piezoelectric plate, rigidly fixed on the cantilever surface, is designated to the mechanical-electrical conversion. Several different

configurations to this basic one have been studied: cantilevers with two piezoelectric plates [4, 5], cantilever in the clamped-clamped configuration with an axial pre-load [6], cantilevers with dynamic magnifier [7], and devices with nonlinear elements [8, 9].

In this work, we model a novel design of a piezoelectric energy harvester. The main idea of our project lies in the fact that such energy harvesters are usually excited by a broadband random mechanical vibrations [10, 11]. Therefore, to collect the larger amount of mechanical vibrations, more frequencies must be equally excitable in the energy harvester in order to have a wide frequency response function. To this end we extend the concept of dynamic magnifier previously discussed in literature [7] by inserting, between the cantilever clamped end and the excited base, a mass-spring-damper system made by a further cantilever with additional piezoelectric plates. Such configuration permits one to both extend the range of excitable frequencies and increase the output voltage produced by the energy harvester. In the first part of this article we review the coupled electromechanical equations which describe the behaviour of piezoelectric materials [12, 13, 14] and we discuss the finite element model used to solve them. Then we describe the design of the energy harvester and we show the electrical outputs under different conditions of piezoelectric plates configurations and external excitations.

2. Model

In this Section, we are going to illustrate and discuss the Finite Element Model (FEM) used to describe the electromechanical behaviour of the piezoelectric energy harvester.

The positive-defined stored energy density U for a piezoelectric material is defined by [12]:

$$dU(\mathbf{S}, \mathbf{D}) = \mathbf{T}^t d\mathbf{S} + \mathbf{E}^t d\mathbf{D} , \quad (1)$$

where \mathbf{S} , \mathbf{T} , \mathbf{E} , and \mathbf{D} are the strain vector, the stress vector, the electric field vector, and the electric displacement vector, respectively, whereas the superscript t indicates the matrix transpose operation. However, the right potential energy to correctly describe the electromechanical coupling is the enthalpy density H , defined as the opposite of the Legendre transform of U , that is:

$$dH(\mathbf{S}, \mathbf{E}) = dU - d(\mathbf{E}^t \mathbf{D}) = d\mathbf{S}^t \mathbf{T} - d\mathbf{E}^t \mathbf{D} , \quad (2)$$

where we used the fact that $d\mathbf{S}^t \mathbf{T} = \mathbf{T}^t d\mathbf{S}$ being the product a scalar quantity. In fact, the assumption of linear responses for mechanical, electrical, and piezoelectrical behaviours leads to:

$$H = \frac{1}{2} \mathbf{S}^t c_p^E \mathbf{S} - \mathbf{S}^t e^t \mathbf{E} - \frac{1}{2} \mathbf{E}^t \varepsilon^S \mathbf{E} , \quad (3)$$

where c_p^E , e , and ε^S are the elastic, piezoelectric, and dielectric constant matrices, respectively. On the other hand, according to Eqs. (2) and (3) we obtain:

$$U = \frac{1}{2} \mathbf{S}^t c_p^E \mathbf{S} + \frac{1}{2} \mathbf{E}^t \varepsilon^S \mathbf{E} , \quad (4)$$

which shows no piezoelectric interactions. However, restrictions on c_p^E and ε^S arise from the positive definiteness of U . The piezoelectric constitutive equations result from Eqs. (2)-(3):

$$\mathbf{T} = \nabla_{\mathbf{S}} H = c_p^E \mathbf{S} - e^t \mathbf{E} , \quad (5)$$

$$\mathbf{D} = -\nabla_{\mathbf{E}} H = e \mathbf{S} + \varepsilon^S \mathbf{E} . \quad (6)$$

To obtain the dynamical equations which describe the electromechanical evolution of the system we will study the problem in the framework of the Euler-Bernoulli beam theory, where the shear stress is neglected as well as the rotational inertia, and we apply the Hamilton's principle of stationary action [15, 16, 14], which attests that the evolution of the system is a solution, under the constraint of stationary endpoints, of the functional equation:

$$\int_{t_1}^{t_2} (\delta L + \delta W) dt = 0 , \quad (7)$$

where δL and δW are the functional variations of the Lagrangian L and external work W , respectively. According to the previous discussion, the correct potential energy that we have to introduce in the Lagrangian is the enthalpy, therefore we have:

$$L = T - H = T - (U_m - U_e) , \quad (8)$$

being T the kinetic energy, U_m the mechanical potential energy, and U_e the electrical potential energy:

$$T = \frac{1}{2} \int_{\mathcal{V}_b} \rho_b \dot{\mathbf{r}}^t \dot{\mathbf{r}} d\mathcal{V}_b + \frac{1}{2} \int_{\mathcal{V}_p} \rho_p \dot{\mathbf{r}}^t \dot{\mathbf{r}} d\mathcal{V}_p , \quad (9)$$

$$U_m = \int_{\mathcal{V}_b} \int_{\mathbf{S}} d\mathbf{S}^t \mathbf{T} d\mathcal{V}_b + \int_{\mathcal{V}_p} \int_{\mathbf{S}} d\mathbf{S}^t \mathbf{T} d\mathcal{V}_p , \quad (10)$$

$$U_e = \int_{\mathcal{V}_p} \int_{\mathbf{E}} d\mathbf{E}^t \mathbf{D} d\mathcal{V}_p , \quad (11)$$

where \mathcal{V} is the volume, ρ the mass density, and \mathbf{r} the mechanical displacement vector, whereas the subscripts b and p stand for the metallic beam layer and the piezoelectric layer, respectively, and the superimpose dot indicates the time derivative. For the piezoelectric layer, we have to insert the constitutive equations (5)-(6) into Eqs. (10)-(11). On the other hand, the relationship between strain and stress in the metallic beam is simply:

$$\mathbf{T} = c_b \mathbf{S} , \quad (12)$$

being c_b the corresponding elastic matrix.

In the following we will explicitly find solutions of Eq. (7) by making us of the FEM applied to the energy harvesting device. Let us initially consider a unimorph piezoelectric energy

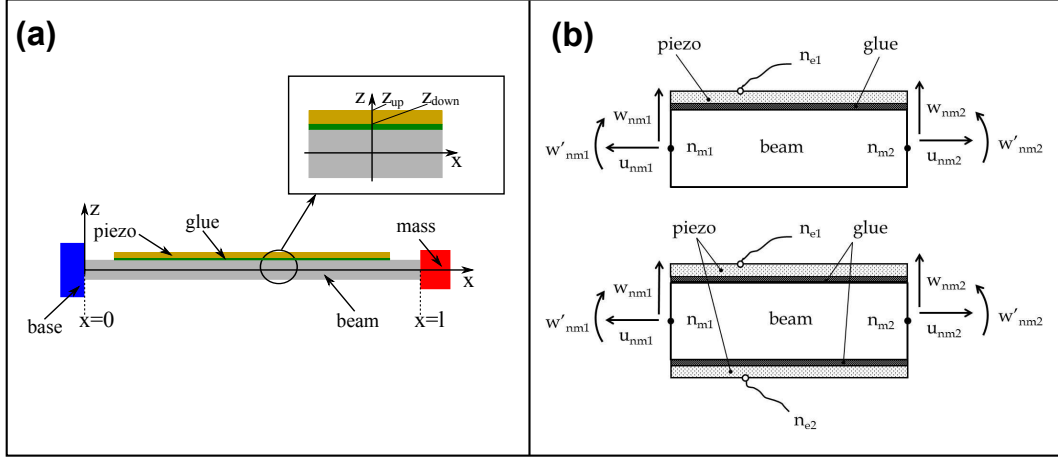


Figure 1. (a) Sketch view of an unimorph piezoelectric energy harvester. The right-oriented Cartesian reference of frame is indicated; $x = 0$ at the base, $x = l$ at the free end, $z = 0$ at the half of the metallic beam thickness. Inset: a magnified view of the part of the device highlighted in the black circle. The positions of z_{up} and z_{down} are indicated. (b) Illustration and characteristic of the element used in the FEM for unimorph (top) and bimorph (bottom) piezoelectric energy harvester. n_{mi} and n_{ei} are the mechanical and the electrical nodes, respectively, whereas $(u_{nmi}, w_{nmi}, w'_{nmi})$ are the deformation along x , the deformation along z , and the rotation around y , respectively, where $i = 1, 2$.

harvester composed by a metallic beam and a piezoelectric plate rigidly fixed on a common surface; in the sequel we will easily extend the obtained formulation to bimorph and multimorph configurations. The beam is constrained with the clamped-free boundary conditions. Moreover, a seismic mass is placed at the tip of the free end. Through the base where the beam is fixed, the energy harvesting device is sensitive to the surrounding vibrations (see Fig. 1-(a)).

The whole beam is characterized by a length l , a width b , and a thickness h equal to either $h = h_b$, where only the metallic beam is present, or $h = h_b + h_g + h_p$, when we have the metallic beam, the piezoelectric plate (h_p) and the epoxy glue (h_g) used to fixed the piezoelectric plate at the metallic beam. A right-oriented Cartesian reference frame is introduced, where the x -axis is along l , the y -axis is along b , and the z -axis is along h . Generally, the mechanical displacements are the translations u, v, w along x, y, z , respectively, and the corresponding rotations u', v', w' , where the superscript $'$ indicates the space derivative with respect to x . However, in first approximation we will consider three contributions only: u (axial deformation), w (flexural deformation), and w' (flexural rotation around y -axis). In order to develop the FEM, the whole beam will be divided into several beam elements whose nodes at the ends are subjected to the considered mechanical displacements (see Fig. 1-(b)); the number of mechanical nodes is n_m . To this goal, we introduce the time-dependent vector of nodal displacements $\Delta_i(t) = (u_1 w_1 w'_1 u_2 w_2 w'_2)^t$, where indexes 1, 2 represent the nodes closer and further to the fixed tip of the beam, respectively, and the dependence on time of u, w, w' is understood. Thus,

the displacements at point x and time t are $\Delta_L(x, t) = N(x)\Delta_i(t)$, where $N(x)$ is the matrix composed by shape functions $N_u(x), N_w(x), N_{w'}(x)$, being L the length of the beam element considered:

$$N_u(x) = \begin{pmatrix} 1 - \frac{x}{L} & 0 & 0 & \frac{x}{L} & 0 & 0 \end{pmatrix}, \quad (13)$$

$$N_w(x) = \begin{pmatrix} 0 & 2\frac{x^3}{L^3} - 3\frac{x^2}{L^2} - 1 & \frac{x^3}{L^2} - 2\frac{x^2}{L} + x & 0 & -2\frac{x^3}{L^3} + 3\frac{x^2}{L^2} & \frac{x^3}{L^2} - \frac{x^2}{L} \end{pmatrix}, \quad (14)$$

$$N_{w'}(x) = \begin{pmatrix} 0 & 6\frac{x^2}{L^3} - 6\frac{x}{L^2} & 3\frac{x^2}{L^2} - 4\frac{x}{L} + 1 & 0 & -6\frac{x^2}{L^3} + 6\frac{x}{L^2} & 3\frac{x^2}{L^2} - 2\frac{x}{L} \end{pmatrix}, \quad (15)$$

$$N(x) = \begin{pmatrix} N_u(x) \\ N_w(x) \\ N_{w'}(x) \end{pmatrix}, \quad (16)$$

where, explicitly, $u(x, t) = N_u(x)\Delta_i(t)$, $w(x, t) = N_w(x)\Delta_i(t)$, $w'(x, t) = N_{w'}(x)\Delta_i(t)$, since $N_{w'}(x) = N_{w'}(x)$. Finally, in order to separate the axial and the flexural behaviours, we write:

$$\Delta_L^{\text{ax}}(x, t) = \begin{pmatrix} u(x) \\ 0 \\ 0 \end{pmatrix} = \begin{pmatrix} N_u(x) \\ \mathcal{O}_{(1,6)} \\ \mathcal{O}_{(1,6)} \end{pmatrix} \Delta_i(t), \quad (17)$$

$$\Delta_L^{\text{flex}}(x, t) = \begin{pmatrix} -z w' \\ 0 \\ w \end{pmatrix} = \begin{pmatrix} -z N_{w'}(x) \\ \mathcal{O}_{(1,6)} \\ N_w \end{pmatrix} \Delta_i(t), \quad (18)$$

since a point at distance z from the axial neutral axis is subjected to a displacement equal to $-z w' = -z N_{w'} \Delta_i$ and $\mathcal{O}_{(1,6)}$ represents a (1×6) zero matrix. The last considerations on the mechanical behaviour involve the strain vector \mathbf{S} , which is determined by the operator matrix Ψ :

$$\Psi = \begin{pmatrix} \partial_x & 0 & 0 \\ 0 & \partial_y & 0 \\ 0 & 0 & \partial_z \\ \partial_y & \partial_x & 0 \\ \partial_z & 0 & \partial_x \\ 0 & \partial_z & \partial_y \end{pmatrix}. \quad (19)$$

according to the relationship $\mathbf{S}(x, t) = \Psi \Delta_L(x, t)$, where we used the simplify notation ∂_i ($i = x, y, z$) to indicate the partial derivative with respect to spatial coordinates. In particular, since we suppose that the axial and the flexural behaviour are not correlated, we have:

$$\mathbf{S}_{\text{ax}} = \Psi \Delta_L^{\text{ax}} = \begin{pmatrix} N_u'(x) \\ \mathcal{O}_{(5,3)} \end{pmatrix} \Delta_i = \Lambda_{\text{ax}}' \Delta_i, \quad (20)$$

$$\mathbf{S}_{\text{flex}} = \Psi \mathbf{\Delta}_L^{\text{flex}} = -z \begin{pmatrix} N_w''(x) \\ \mathcal{O}_{(5,3)} \end{pmatrix} \mathbf{\Delta}_i = -z \Lambda_{\text{flex}}'' \mathbf{\Delta}_i , \quad (21)$$

being $\mathcal{O}_{(5,3)}$ a (5×3) zero matrix.

The electrical behaviour of a single piezoelectric layer is determined by the electric field vector \mathbf{E} , defined as the opposite of the gradient of the electric potential inside the layer, that is, $\mathbf{E} = -\nabla\varphi$. On the other hand, the electric potential can be conveniently written by making use of the shape function $N_v(z)$ as:

$$\varphi(z, t) = N_v(z)V(t) = \frac{z - z_{\text{down}}}{z_{\text{up}} - z_{\text{down}}} V(t) , \quad (22)$$

where we imposed the null potential at the lower surface of the piezoelectric layer (see Fig. 1-(a) for position of z_{up} and z_{down}). According to these considerations, the electric potential will be:

$$\mathbf{E} = - \begin{pmatrix} \partial_x \\ \partial_y \\ \partial_z \end{pmatrix} N_v(z)V(t) = - \begin{pmatrix} 0 \\ 0 \\ N_v'(z) \end{pmatrix} V(t) = -\Lambda_v'(z)V(t) , \quad (23)$$

where here the superscript $'$ indicates the space derivative with respect to z . Since two conductive electrodes are placed on both surfaces of the piezoelectric layer, all the piezoelectric elements generate the same voltage, thus we consider just one electrical node n_e for each piezoelectric layer. In other words, the electric potential V is a scalar.

We highlight that each beam element of the FEM is either a single layer, when only the metallic beam is present, or a multilayer, when both the metallic beam and the piezoelectric layer are present. Furthermore, in the second case we neglect the dynamical effects produced by the glue layer; the only contribution of the glue layer will be found in the computation of z_{up} and z_{down} (see Eq. (22)).

By making explicit the Lagrangian term into Eq. (7) we obtain:

$$\int_{t_1}^{t_2} (\delta T - \delta U_m + \delta U_e + \delta W) dt = 0 , \quad (24)$$

where the various terms must be computed for each element and subsequently assembled together in order to describe the whole structure. Therefore, by overwriting the symbol \sim to the quantities referring to a single element of the FEM we have that the kinetic energy is:

$$\delta \tilde{T} = \int_{\mathcal{V}_b} \rho_b (\delta \dot{u} \dot{u} + \delta \dot{w} \dot{w}) d\mathcal{V}_b + \int_{\mathcal{V}_p} \rho_p (\delta \dot{u} \dot{u} + \delta \dot{w} \dot{w}) d\mathcal{V}_p = \delta \dot{\mathbf{\Delta}}_i^t \left(\widetilde{M}_b + \widetilde{M}_p \right) \dot{\mathbf{\Delta}}_i , \quad (25)$$

where the mass matrices are:

$$\widetilde{M}_j = \int_{\mathcal{V}_j} \rho_j (N_u^t N_u + N_w^t N_w) d\mathcal{V}_j, \quad j = b, p. \quad (26)$$

By making use of Eqs. (5), (12), (20), and (21) we obtain:

$$\begin{aligned} \delta \tilde{U}_m &= \int_{\mathcal{V}_b} \mathbf{S}^t d\mathbf{T} d\mathcal{V}_b + \int_{\mathcal{V}_p} \mathbf{S}^t d\mathbf{T} d\mathcal{V}_p = \\ &= \int_{\mathcal{V}_b} (\mathbf{S}_{\text{ax}}^t d\mathbf{T}_{\text{ax}} + \mathbf{S}_{\text{flex}}^t d\mathbf{T}_{\text{flex}}) d\mathcal{V}_b + \int_{\mathcal{V}_p} (\mathbf{S}_{\text{ax}}^t d\mathbf{T}_{\text{ax}} + \mathbf{S}_{\text{flex}}^t d\mathbf{T}_{\text{flex}}) d\mathcal{V}_p = \\ \delta \Delta_i^t \left(\tilde{K}_b^{\text{ax}} + \tilde{K}_p^{\text{ax}} + \tilde{K}_b^{\text{flex}} + \tilde{K}_p^{\text{flex}} \right) \Delta_i - \delta \Delta_i^t \left(\tilde{\Theta}_p^{\text{flex}} - \tilde{\Theta}_p^{\text{ax}} \right) V &= \delta \Delta_i^t \left(\tilde{K} \Delta_i - \tilde{\Theta} V \right), \quad (27) \end{aligned}$$

where the axial stiffness matrix, the flexural stiffness matrix, the axial electro-mechanical coupling matrix, and the flexural electro-mechanical coupling matrix are respectively given by:

$$\tilde{K}_j^{\text{ax}} = \int_{\mathcal{V}_j} \Lambda_{\text{ax}}^t c_j^E \Lambda_{\text{ax}}' d\mathcal{V}_j \quad (28)$$

$$\tilde{K}_j^{\text{flex}} = \int_{\mathcal{V}_j} z^2 \Lambda_{\text{flex}}^t c_j^E \Lambda_{\text{flex}}'' d\mathcal{V}_j \quad (29)$$

$$\tilde{\Theta}_p^{\text{ax}} = \int_{\mathcal{V}_p} \Lambda_{\text{ax}}^t e^t \Lambda_v' d\mathcal{V}_p \quad (30)$$

$$\tilde{\Theta}_p^{\text{flex}} = \int_{\mathcal{V}_p} z \Lambda_{\text{flex}}^t e^t \Lambda_v' d\mathcal{V}_p, \quad (31)$$

being $j = b, p$ and $c_b^E \equiv c_b$, whereas $\tilde{K} = \tilde{K}_b^{\text{ax}} + \tilde{K}_p^{\text{ax}} + \tilde{K}_b^{\text{flex}} + \tilde{K}_p^{\text{flex}}$ is the total stiffness matrix and $\tilde{\Theta} = \tilde{\Theta}_p^{\text{flex}} - \tilde{\Theta}_p^{\text{ax}}$ is the total electro-mechanical coupling matrix.

Finally, by using Eq. (6) we have:

$$\begin{aligned} \delta \tilde{U}_e &= \int_{\mathcal{V}_p} d\mathbf{E}^t \mathbf{D} d\mathcal{V}_p = \int_{\mathcal{V}_p} d\mathbf{E}^t [e (\mathbf{S}_{\text{ax}} + \mathbf{S}_{\text{flex}}) + \varepsilon^S \mathbf{E}] d\mathcal{V}_p = \\ \delta V^t \left(\tilde{\Theta}_p^{\text{flex}} - \tilde{\Theta}_p^{\text{ax}} \right)^t \Delta_i + \delta V^t \tilde{C}_p V &= \delta V^t \left(\tilde{\Theta}^t \Delta_i + \tilde{C}_p V \right), \quad (32) \end{aligned}$$

where:

$$\tilde{C}_p = \int_{\mathcal{V}_p} \Lambda_v^t \varepsilon^S \Lambda_v' d\mathcal{V}_p, \quad (33)$$

is the capacitance matrix. We finally remark that in the volume integrals the terms z and z^2 lead to static moments and inertia moments of the section, respectively. By assembling the element matrices we obtain the global matrices which appear in the global equations of motion: Δ is the $(3n_m \times 1)$ global displacement vector, M is the $(3n_m \times 3n_m)$ global mass matrix, K is the $(3n_m \times 3n_m)$ global stiffness matrix, Θ is the $(3n_m \times n_e)$ global electromechanical coupling matrix, and C_p is the $(n_e \times n_e)$ diagonal global capacitance matrix, being 3 the number of degrees of freedom of each mechanical node. However, since we consider an unimorph

piezoelectric energy harvester, we have $n_e = 1$, thus Θ is a vector and C_p is a scalar. Therefore we have:

$$\delta T = \delta \dot{\Delta}^t M \dot{\Delta} , \quad (34)$$

$$\delta U_m = \delta \Delta^t (K \Delta - \Theta V) , \quad (35)$$

$$\delta U_e = \delta V (\Theta^t \Delta + C_p V) . \quad (36)$$

The seismic mass, placed at the free end of the beam, is introduced in the model as a lumped mass whose inertial characteristics (mass and inertia moment) are added in the mass matrix M at the corresponding degrees of freedom.

The external work W_L applied to a single element is:

$$W_L = \Delta_L^t \mathbf{F}_L + \varphi Q , \quad (37)$$

where \mathbf{F}_L is the vector of external forces and Q is the charge generated by the piezoelectric layer. After substitution of Δ_L and φ according to their expressions in terms of Δ_i and V we obtain $W_L = \Delta_i^t N^t \mathbf{F}_L + V^t N_v^t Q$. By assembling the element matrices and by remarking that N_v must be computed at $z = z_{up}$ since we are interested in the potential at the surface, that is, $N_v = 1$ (see Eq. (22)), we obtain the external work acting on the whole structure:

$$W = \Delta^t \mathbf{F} + V^t Q . \quad (38)$$

By substituting Eqs. (34)-(38) in Eq. (24) and by integrating under the constraint $\delta \Delta(t_1) = \delta \Delta(t_2) = 0$ (hypothesis of stationary endpoints) we finally obtain:

$$M \ddot{\Delta}_i + K \Delta_i - \Theta V = \mathbf{F} , \quad (39)$$

$$\Theta^t \Delta_i + C_p V + Q = 0 . \quad (40)$$

Let us now improve the model by making three considerations. (I) In common applications, the electrodes of the piezoelectric element are connected to an external resistance R and \dot{Q} represents the current generated, given by $\dot{Q} = V/R$. (II) Mechanical damping effects can be taken into account by considering the Rayleigh dissipation function:

$$\mathcal{R} = \frac{1}{2} \dot{\Delta}^t C_{qq} \dot{\Delta} , \quad (41)$$

where C_{qq} is the phenomenological damping matrix. (III) In energy harvesting applications the motion of the beam is due to acceleration of the base $\ddot{\Delta}_b$, whereas the external forces \mathbf{F} are null.

Under all these considerations, the complete electromechanical equations become:

$$M \ddot{\Delta} + C_{qq} \dot{\Delta} + K \Delta - \Theta V = -M \ddot{\Delta}_b , \quad (42)$$

$$\Theta^t \dot{\Delta} + C_p \dot{V} + \frac{V}{R} = 0 , \quad (43)$$

If we consider a bimorph piezoelectric energy harvester, realized by a metallic beam bracketed between two piezoelectric layers, we have to increase the number of electrical nodes, that is, $n_e = 2$, since we must take into account the voltage generated by both piezoelectric plates. Therefore, the voltage becomes the two-elements vector $V = (V_1 \ V_2)^t$, whereas Θ and C_p become a $(3n_m \times 2)$ and (2×2) matrices, respectively equal to $\Theta = (\Theta_1 \ \Theta_2)$ and $C_p = \text{diag}(C_{p1}, C_{p2})$, being V_1, V_2 the voltages of the two piezoelectric layers and Θ_1, Θ_2 and C_{p1}, C_{p2} the corresponding electromechanical coupling vectors and capacitances, respectively, whereas “diag()” defines a diagonal matrix. However, in applications we need just one value of voltage exiting from the energy harvester. Such condition is obtain by connecting the two piezoelectric layers either in series to maximize the voltage or in parallel to maximize the current; in particular, in the first case the two piezoelectric plates are poled in antiparallel directions, whereas in the second case they are poled in parallel directions. We remark that the condition of antiparallel polarization is obtain by writing the piezoelectric constants with opposite sign. In order to carry out a single value of voltage, let us split Eq. (43) by explicitly showing the behaviour of two piezoelectric plates and by restoring the output charge:

$$M \ddot{\Delta} + C_{qq} \dot{\Delta} + K \Delta - (\Theta_1 V_1 + \Theta_2 V_2) = -M \ddot{\Delta}_b, \quad (44)$$

$$\Theta_1^t \dot{\Delta} + C_{p1} \dot{V}_1 + \dot{Q}_1 = 0, \quad (45)$$

$$\Theta_2^t \dot{\Delta} + C_{p2} \dot{V}_2 + \dot{Q}_2 = 0, \quad (46)$$

being Q_1, Q_2 the output charges generated by the piezoelectric plates. Figure 2 shows the configurations for series (a) and parallel (b) connection. In series connection, the global output charge is equal to each output charge generated by each piezoelectric plates, $Q = Q_1 = Q_2$, whereas the global output voltage is the sum of each output voltage, that is, $V = V_1 + V_2$; in terms of electrical current I flowing through the external load R we have $I = \dot{Q} = V/R = (V_1 + V_2)/R$. At this point we sum Eq. (45) to Eq. (46) under the assumption of equal piezoelectric materials, that is, $C_{p1} = C_{p2}$ and $V_1 = V_2$, leading to:

$$M \ddot{\Delta} + C_{qq} \dot{\Delta} + K \Delta - \Theta V = -M \ddot{\Delta}_b, \quad (47)$$

$$\Theta^t \dot{\Delta} + C_p \dot{V} + \frac{V}{R} = 0, \quad (48)$$

where:

$$C_p = \frac{C_{p1}}{2} = \frac{C_{p2}}{2}, \quad \Theta = \frac{\Theta_1 + \Theta_2}{2}. \quad (49)$$

Conversely, in parallel connection the global output charge is the sum of each output charge generated by each piezoelectric plates, $Q = Q_1 + Q_2$, whereas the global output voltage is equal to each output voltage, that is, $V = V_1 = V_2$. By following the same procedure discussed for series connection (the assumption of equal piezoelectric materials is not necessary) we obtain:

$$M \ddot{\Delta} + C_{qq} \dot{\Delta} + K \Delta - \Theta V = -M \ddot{\Delta}_b, \quad (50)$$

$$\Theta^t \dot{\Delta} + C_p \dot{V} + \frac{V}{R} = 0, \quad (51)$$

where:

$$C_p = C_{p1} + C_{p2}, \quad \Theta = \Theta_1 + \Theta_2 . \quad (52)$$

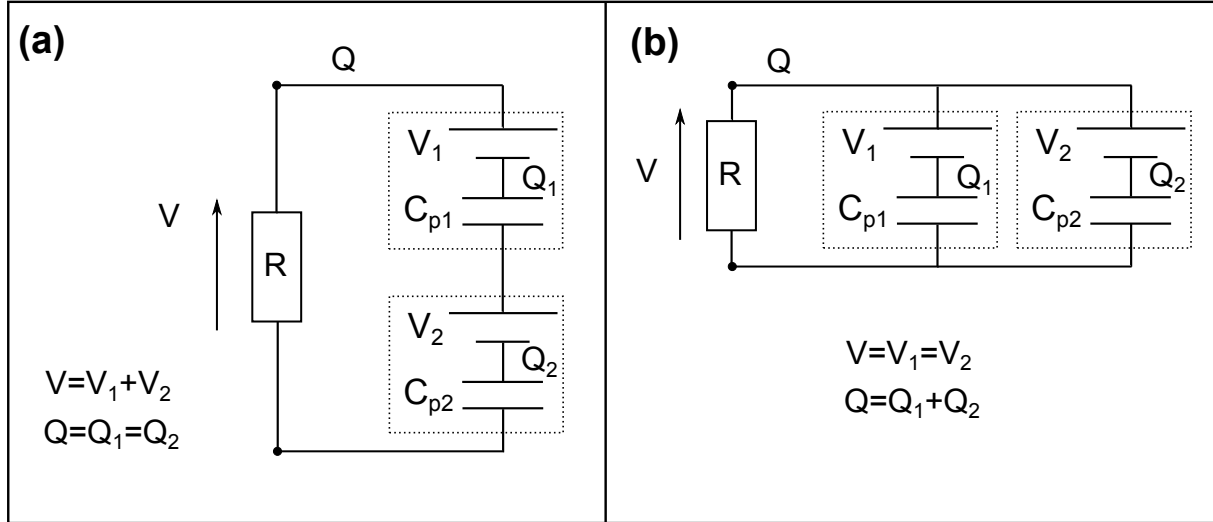


Figure 2. (a) Series connection of two piezoelectric plates. (b) Parallel connection of two piezoelectric plates. V_i , C_{pi} , and Q_i ($i = 1, 2$) are the voltage, capacitance, and charge of each piezoelectric plate, respectively, V and Q represent the global output voltage and output charge, respectively, R is the external load.

On the other hand, if more bimorph piezoelectric energy harvesters are mechanically connected together we will follow the same rules to insert the correct matrices into the electromechanical equations:

series connection $\Theta = \sum_i \Theta_i / 2$ and $1/C_p = \sum_i 1/C_{pi}$

parallel connection $\Theta = \sum_i \Theta_i$ and $C_p = \sum_i C_{pi}$

where the sum is extended to all the piezoelectric plates whereas Θ_i and C_{pi} represent the electromechanical coupling vectors and capacitances of each piezoelectric plates, respectively. We remark that for series connection the two piezoelectric plates of a single cantilever are always poled in opposite directions.

3. Design and electrical performance

Piezoelectric energy harvesters made up by a single cantilever, as sketched in Fig. 1, are easily realizable, but they are basically inconvenient when one needs to collect the energy arising from vibrations with a large frequency spectrum. In fact, such energy harvesters show good but narrow resonances around their natural frequencies which generally differ each other by at least one order of magnitude. In order to deal with this limit and to increase the power generated by the energy harvester, Aladwani *et al.* [7] provided the cantilevered harvester with a spring-mass

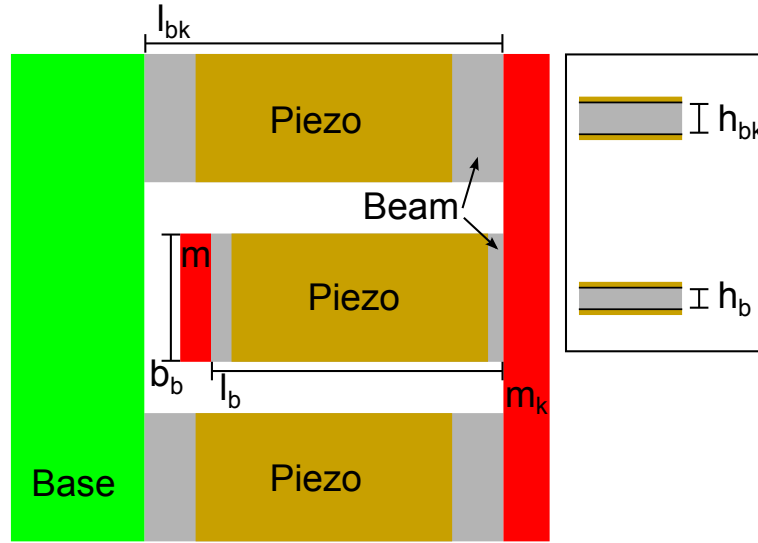


Figure 3. Schematic top view of the energy harvester. Green base: link between the energy harvester and the environmental vibrations; grey parts: metallic beams; brown parts: piezoelectric plates; red parts: lumped masses. Inset: transversal sections of dynamic magnifier (up) and main cantilever (down). l_{bk} , b_{bk} , h_{bk} and l_b , b_b , h_b are the length, the width, and the thickness of the dynamic magnifier and the main cantilever, respectively, whereas m_k and m are the seismic masses of the dynamic magnifier and the main cantilever, respectively.

system, called dynamic magnifier, placed between the piezoelectric cantilever and the vibrating base. Through theoretical considerations and numerical examples they proved that by properly adjusting the parameters of the dynamic magnifier the harvested power and the effective bandwidth can be significantly improved. This type of configuration operates with the same principles, but in the opposite ways, of the dynamic vibration absorber, commonly discussed as application in vibrating systems (see [17] for details). In particular, the spring-mass system considered is simply composed by a perfect spring (constant stiffness acting on one direction only) connected to a lumped mass. Nevertheless, we know that such idealized system shows several technical limitations to be realized. Therefore, we extend the main idea proposed by Aladwani *et al.* by developing an active dynamic magnifier, able to produce useful power itself.

The piezoelectric energy harvester here developed is sketched in Fig. 3. It consists of two parallel metallic beams fixed, on one end, to the vibrating base; furthermore they are connected together with a metallic bar fixed on their free ends. Between these two beams, and on the same plane, a third beam is fixed on one end at the same bar; on the free end it supports a seismic mass. On the resulting six surfaces of all the metallic beams we rigidly fixed piezoelectric plates. The two parallel beams and the metallic bar represent the dynamic magnifier, whereas the central beam and its seismic mass are the main cantilever. Thanks to this design, the dynamic magnifier acquires a double role: it improves the power and the bandwidth of the main cantilever, as proved in [7], and it generates itself power thanks to the piezoelectric plates placed on it. Table

1 shows the whole geometrical and material properties of the energy harvester. In particular, we have considered aluminum beam, whereas the piezoelectric plates are the commercial PIC 155 of Physik Instrumente. In the FEM, both the bar of the dynamic magnifier and the seismic mass of the main cantilever are modeled as lumped masses since they do not significantly change the deformation of cantilevers.

Length of dynamic magnifier beam l_{bk}	70 mm
Width of dynamic magnifier beam b_{bk}	25 mm
Thickness of dynamic magnifier beam h_{bk}	3 mm
Length of main cantilever beam l_b	57 mm
Width of main cantilever beam b_b	25 mm
Thickness of main cantilever beam h_b	2 mm
Mass of dynamic magnifier bar m_k	50 g
Mass of main cantilever seismic mass m	10 g
Length of piezoelectric plates l_p	50 mm
Width of piezoelectric plates b_p	25 mm
Thickness of piezoelectric plates h_p	0.5 mm
Distance piezoelectric plate - clamped end in dynamic magnifier	10 mm
Distance piezoelectric plate - clamped end in main cantilever	3 mm
Glue thickness	0.15 mm
Mass density of beams (Al) ρ_b	2710 kg/m ³
Young's modulus of beams (Al) E_b	73.1 GPa
Mass density of piezoelectric plates ρ_p	7800 kg/m ³
d_{31}	-165×10^{-12} C/N
d_{33}	360×10^{-12} C/N
s_{11}^E	15.6×10^{-12} m ² /N
s_{33}^E	19.7×10^{-12} m ² /N
ε_{11}^T	$1400 \varepsilon_0$
ε_{33}^T	$1500 \varepsilon_0$

Table 1. Geometrical and material properties of the energy harvester.

Let us discuss how the whole dynamics is influenced by the presence of the dynamic magnifier. The single main cantilever, fixed on its clamped end at the vibrating base, shows the following natural frequencies: $f_{MC1} = 347.2$ Hz and $f_{MC2} = 3233.1$ Hz. As required by the analysis of Aladwani *et al.*, the dynamic magnifier has been designed in order to present natural frequencies closer to those ones of the main cantilever: $f_{DM1} = 234.1$ Hz and $f_{DM2} = 2728.8$ Hz. The combination of these two parts in the final set up leads to an energy harvester whose the first three natural frequencies are: $f_1 = 224.1$ Hz, $f_2 = 302.3$ Hz, and $f_3 = 2809.2$ Hz. In particular, the corresponding modal shapes are shown in Fig. 4.

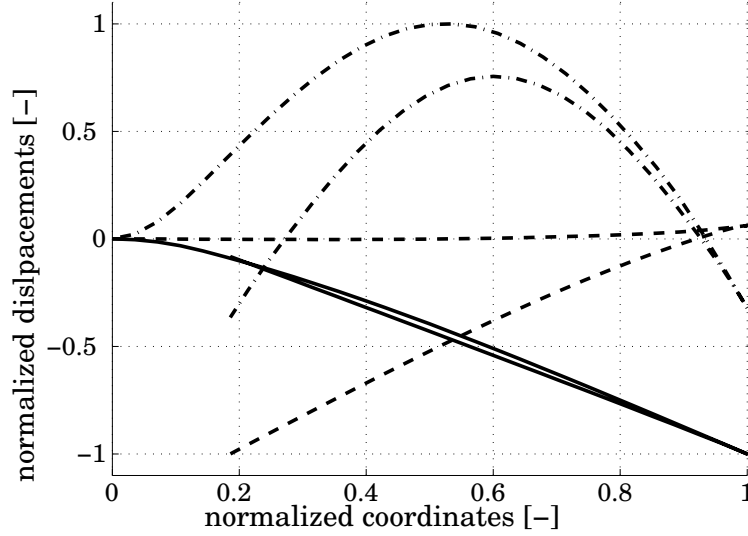


Figure 4. Modal shapes of the energy harvester. Frequencies are obtained in the short-circuit configuration. Solid line: $f_1 = 224.1$ Hz; dashed line: $f_2 = 302.3$ Hz; dash-dot line: $f_3 = 2809.2$ Hz.

We highlight that the frequencies previously reported are obtained by considering the piezoelectric plates in the short-circuit configuration. Physically, this means that the piezoelectric materials influence the device's stiffness only through their intrinsic structure, without any piezoelectric effect (since no charges are collected on the electrode surfaces, no voltage and consequently no additional stress is present). Conversely, when the piezoelectric plates are in the open-circuit configuration, the additional stress, due to the piezoelectric effect, stiffens the whole structure, leading to higher natural frequencies: $f_1 = 233.3$ Hz, $f_2 = 343.2$ Hz, and $f_3 = 2867.0$ Hz.

The electrical response of the energy harvester is obtained by connecting all the piezoelectric plates together and then to an external load, here represented by the resistance R . In the sequel, for sake of simplicity we will consider only the series connection for the piezoelectric elements. We remark that at this stage of our theoretical description we are not able to include a correct value for the damping factors. In fact, such values, because of their phenomenological nature, can be determined only through the comparison between the theoretical predictions and the experimental results, which are not available at this time. Moreover, we cannot use the corresponding values found in literature (see for example [4]) since they refer to different devices. Therefore, all the subsequent analysis will be developed without considering the mechanical damping; the only dissipative mechanism which affects the system is external load.

As first result we show in Fig. 5 the transfer function of the whole energy harvester, compared to the transfer function of the main cantilever only, where an external load of $1\text{ k}\Omega$ is considered. The input signal is the base acceleration oriented along the z -axis, i.e., perpendicular to the piezoelectric plates, whereas the output is the generated voltage. In the frequency

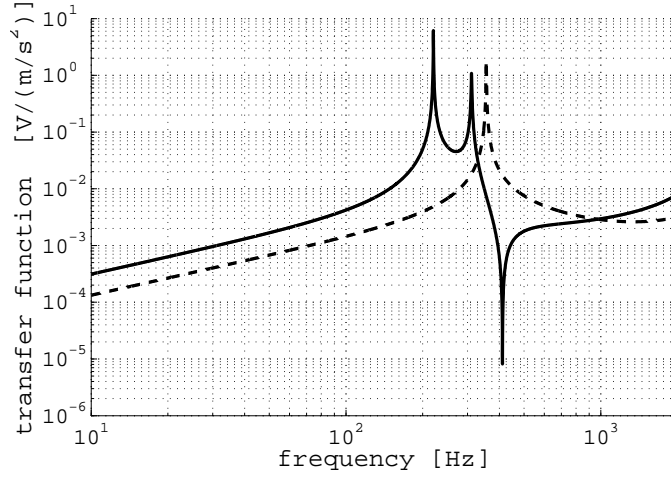


Figure 5. Modulus of the transfer function of the system: the input is the acceleration along the z -axis, the output is the voltage generated with $R = 1 \text{ k}\Omega$. Solid line: complete energy harvester; dashed line: main cantilever only.

domain we have:

$$V(\omega) = H(\omega)\ddot{\Delta}_b(\omega) , \quad (53)$$

where $H(\omega)$ is the corresponding (complex) transfer function of the system. The transfer function H of the complete device is peaked around the frequencies $f_1 = 224.1 \text{ Hz}$, $f_2 = 302.3 \text{ Hz}$, corresponding to the first two natural frequencies in the short-circuit configuration; the value of R considered is relatively very small and it does not significantly affect the mentioned configuration. Similarly, the transfer function H_{MC} of the main cantilever only shows a peak in correspondence of $f_{MC1} = 347.2 \text{ Hz}$. However, as expected by the introduction of the dynamic magnifier, H is wider than H_{MC} around its maximum, proving therefore a larger bandwidth of excitable frequencies. Furthermore, H is basically larger than H_{MC} thanks to the application of piezoelectric elements in the dynamic magnifier.

In order to predict the voltage and the power generated by the energy harvester, we compute the output signal when the device is subjected to random external vibrations. In particular, we assume that such vibrations have a root-mean-square value of the acceleration equal to $a_{\text{rms}} = 20g$, arising from a Power Spectral Density (PSD) constant and null outside the frequency interval $10 \text{ Hz} - 2 \text{ kHz}$; this type of PSD is commonly observed in aerospace applications. The theory of random signals [17] attests that, given the PSD of the input $S_{\text{in}}(\omega)$, the PSD of the output $S_{\text{out}}(\omega)$ is obtained from the relation:

$$S_{\text{out}}(\omega) = |H(\omega)|^2 S_{\text{in}}(\omega) . \quad (54)$$

Since in our case $S_{\text{in}} = S_b$ and $S_{\text{out}} = S_V$, the output signals are:

$$V_{\text{rms}} = \sqrt{\int_0^\infty S_V(\omega) d\omega}, \quad P_{\text{rms}} = \frac{V_{\text{rms}}^2}{R} . \quad (55)$$

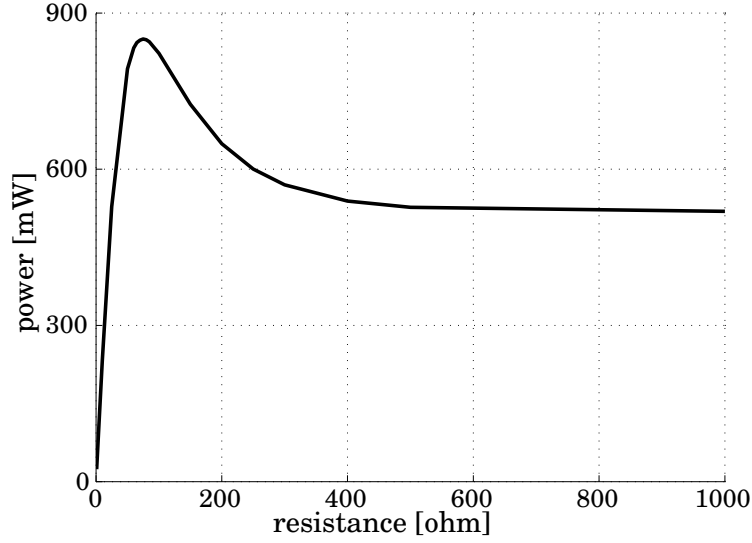


Figure 6. Power P_{rms} generated by the energy harvester under varying external resistance and random external vibration with acceleration $a_{\text{rms}} = 20g$.

As first result, we highlight that the complete device significantly produces more voltage and power with respect to the main cantilever only. Under the same conditions of external excitations and with an external load of $1 \text{ k}\Omega$, the energy harvester produces $V_{\text{rms}} = 22.8 \text{ V}$ and $P_{\text{rms}} = 519 \text{ mW}$, whereas the main cantilever stops at $V_{\text{rms}} = 10.1 \text{ V}$ and $P_{\text{rms}} = 102 \text{ mW}$. A more detailed analysis is shown in Fig. 6 where we plotted the computed root-mean-squared value of the generated power under varying values of the external resistance R . It is clear from these results that the power exhibits a maximum of 800 mW around 100Ω of external load, and then decreases at the value of 520 mW , approximately constant for several values of resistance (up to $10 \text{ M}\Omega$). This analysis shows that the proposed energy harvester is able to power different types of sensors, providing the external vibrations are strong enough.

As final analysis, we computed the dynamical response of the energy harvester when it is subjected to an acceleration pulse $a(t)$ whose PSD corresponds to the previous one considered (constant in a limited bandwidth). Through the Fourier analysis, we obtain that the behaviour of the external pulse in the time domain is [18]:

$$a(t) = A_0 \left[\omega_b \frac{\sin(\omega_b t)}{\omega_b t} - \omega_a \frac{\sin(\omega_a t)}{\omega_a t} \right], \quad (56)$$

where $\omega_i = 2\pi f_i$ ($i = a, b$), being f_a and f_b the lower and the higher frequency of the bandwidth limited white noise considered, respectively, whereas A_0 is the constant amplitude which is set by considering that, by definition:

$$a_{\text{rms}} = \sqrt{\frac{1}{T} \int_0^T a^2(t) dt}, \quad (57)$$

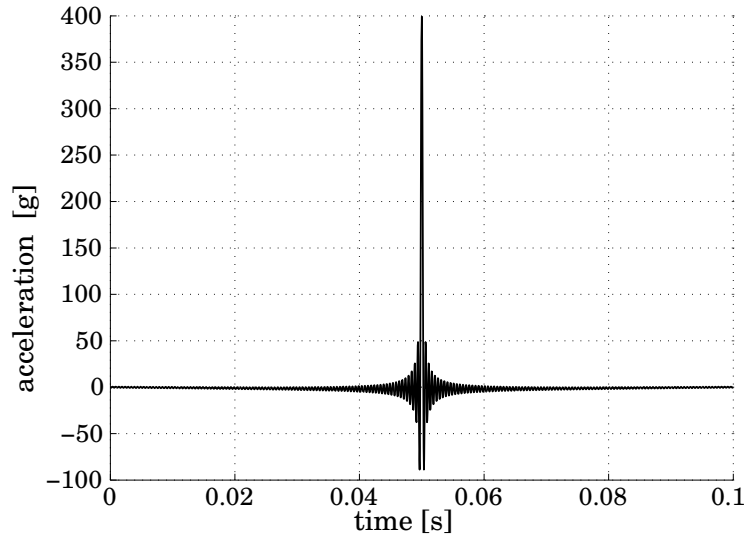


Figure 7. Behaviour of the acceleration pulse used to study the dynamical response of the energy harvester.

where T is the time duration of the signal. The behaviour of the acceleration pulse, given by Eq. (56) with $a_{\text{rms}} = 20g$, is shown in Fig. 7.

The dynamical response of the energy harvester to this type of external excitation is shown in Fig. 8, where we used the value $R = 1 \text{ k}\Omega$. In all the three plots (vertical displacement of the main cantilever free end at the top, voltage generated in the center, power generated at the bottom) we can observe the maximum of the response in correspondence of the highest peak of the excitation, around $t = 0.05 \text{ s}$, followed by damped oscillations. The behaviour of such oscillations arises from the combination of the first two close natural frequencies of the energy harvester, f_1 and f_2 , whereas, as previously remarked, the damping effects are exclusively caused by the dissipation through the external resistance.

4. Conclusions

In this work we have described a piezoelectric energy harvester with an innovative shape, developed in order to enlarge the excitation bandwidth and increase the generated voltage and power. In the first part we have extensively discussed the unidimensional finite element model used to solve the coupled matrix equations which describe the electromechanical behaviour of the energy harvester. In particular, we have shown how such equations are changed when more piezoelectric elements are connected together, by both series and parallel connection. In the second part of the article we have described the design of the proposed piezoelectric energy harvester by highlighting the main innovations brought with respect to similar devices discussed in literature. Finally, we have computed the electrical response of our system when excited by external random vibrations, characterized by a constant an bandwidth limited white noise. The obtained results have shown that this piezoelectric energy harvester can correctly

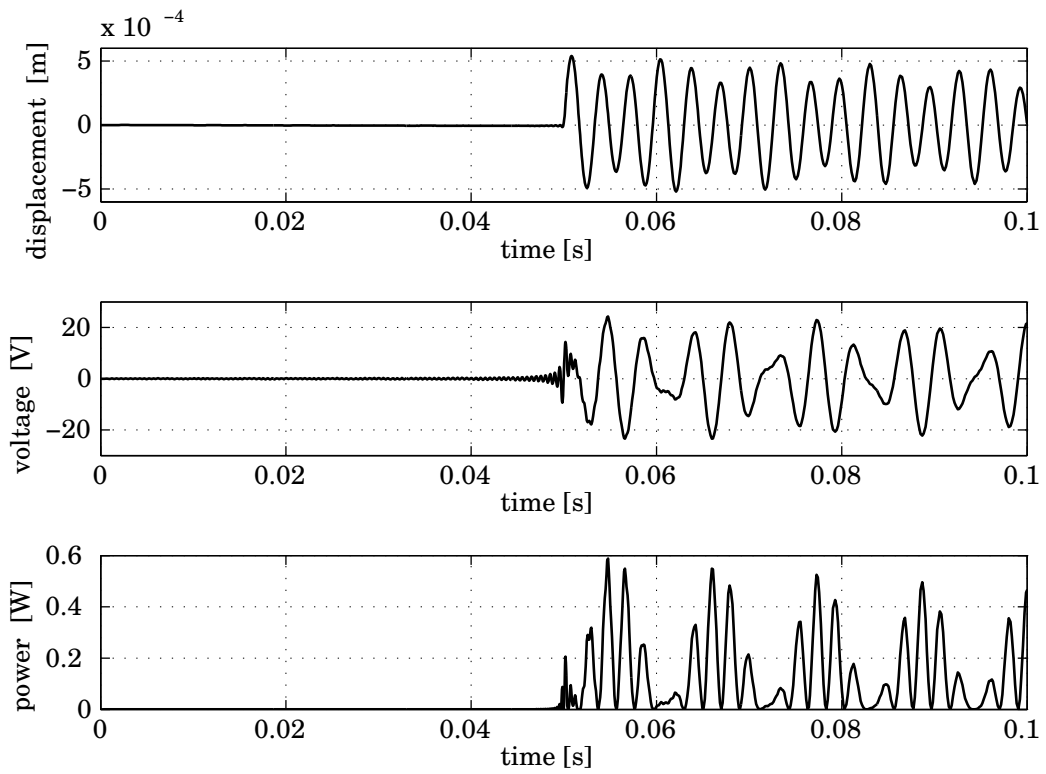


Figure 8. Dynamical response of the energy harvester to the acceleration pulse described by Eq. (56). Top: vertical displacement of the main cantilever free end. Center: voltage generated. Bottom: power generated. External load: $R = 1 \text{ k}\Omega$.

power different types of sensors, especially in aerospace applications.

References

- [1] S.P. Beeby, M.J. Tudor, and N.M. White. Energy harvesting vibration sources for microsystems applications. *Measurement Science and Technology*, 17:R175, 2006.
- [2] A. Erturk and D. J. Inman. Issues in mathematical modeling of piezoelectric energy harvesters. *Smart Materials and Structures*, 17:065016, 2008.
- [3] M Ferrari, V. Ferrari, D. Marioli, and A. Taroni. Modeling, fabrication and performance measurements of a piezoelectric energy converter for power harvesting in autonomous microsystems. *IEEE Transactions on Instrumentation and Measurement*, 55:2096, 2006.
- [4] A. Erturk and D. J. Inman. An experimentally validated bimorph cantilever model for piezoelectric energy harvesting from base excitations. *Smart Materials and Structures*, 18:025009, 2009.
- [5] Q. Ou, X.Q. Chen, S. Gutschmidt, A. Wood, N. Leigh, and A.F. Arrieta. An experimentally validated double-mass piezoelectric cantilever model for broadband vibration-based energy harvesting. *Journal of Intelligent Material Systems and Structures*, 23:117, 2012.
- [6] E.S. Leland and P.K. Wright. Resonance tuning of piezoelectric vibration energy scavenging generators using compressive axial preload. *Smart Materials and Structures*, 15:1413, 2006.
- [7] A. Aladwani, M. Arafa, O. Aldraihem, and A. Baz. Cantilevered piezoelectric energy harvester with a dynamic magnifier. *Journal of Sound and Vibration*, 134:031004, 2012.
- [8] V.R. Challa, M.G. Prasad, Y. Shi, and F.T. Fisher. A vibration energy harvesting device with bidirectional resonance frequency tunability. *Smart Materials and Structures*, 17:015035, 2008.
- [9] R. Masana and M.F. Daqaq. Electromechanical modeling and nonlinear analysis of axially loaded energy harvesters. *Journal of Vibration and Acoustics*, 133:011007, 2011.
- [10] E. Lefeuvre, A. Badel, C. Richard, and D. Guyomar. Energy harvesting using piezoelectric materials: Case of random vibrations. *Journal of Electroceramics*, 18:025009, 2009.
- [11] S. Adhikari, M.I. Friswell, and D.J. Inman. Piezoelectric energy harvesting from broadband random vibrations. *Smart Materials and Structures*, 18:115005, 2009.
- [12] *IEEE Standard on Piezoelectricity 176-1987*, 1987.

- [13] A. Erturk and D. J. Inman. A distributed parameter electromechanical model for cantilevered piezoelectric energy harvesters. *Journal of Vibration and Acoustics*, 130:041002, 2008.
- [14] C. De Marqui Junior, A. Erturk, and D. J. Inman. An electromechanical finite element model for piezoelectric energy harvester plates. *Journal of Sound and Vibration*, 327:9–25, 2009.
- [15] V. I. Arnold. *Mathematical Methods of Classical Mechanics*. Springer, 1989.
- [16] H. A. Sodano, G. Park, and D. J. Inman. Estimation of electric charge output for piezoelectric energy harvesting. *Strain*, 40:49–58, 2004.
- [17] G. Genta. *Vibration Dynamics and Control*. Springer, 2008.
- [18] A. de Sa. *Electronics for scientists*. Prentice Hall, 1997.